Journal of Materials Chemistry A

Accepted Manuscript

ROYAL SOCIETY OF CHEMISTRY

www.rsc.org/materialsA

Table of Contents

Heterogeneous Rhodium-Tin Nanoparticles: Highly Active and Durable Electrocatalysts for the Oxidation of Ethanol

Minjeh Ahn,[a] In Young Cha,[b] Joong Kee Lee,[a] Sung Jong Yoo*[b] and Yung-Eun Sung*[cd]

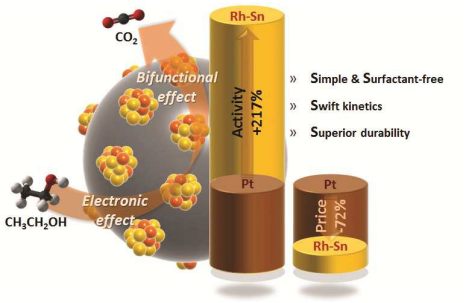

Highly active and durable heterogeneous Rh–Sn nanoparticles for the electrocatalytic oxidation of ethanol have been synthesized using a simple and facile surfactant-free microwave-assisted method.

Journal Name

COMMUNICATION

Heterogeneous Rhodium-Tin Nanoparticles: Highly Active and Durable Electrocatalysts for the Oxidation of Ethanol

Received 00th January 20xx,
Accepted 00th January 20xx

DOI: 10.1039/x0xx00000x

www.rsc.org/MaterialsA

Minjeh Ahn,[a] In Young Cha,[b] Joong Kee Lee,[a] Sung Jong Yoo*[b] and Yung-Eun Sung*[cd]

Facile synthesis of Rh-Sn catalyst for the electrocatalytic oxidation of ethanol is developed via a surfactant-free microwave-assisted method. Bifunctional mechanism and electronic modification with C-C bond splitting enable this electrocatalyst to be remarkbly active and durable at high fuel concentrations, which allows for a significant reduction in volume and weight of the fuel cell system.

Ethanol is an attractive fuel in fuel-cell technology because it is more easily stored and transported than gaseous fuels, and because it is less toxic and more energy-dense than other liquid fuels.[1] Moreover, ethanol is abundant: it can be obtained from sugar- and cellulose-containing raw materials and from inedible plants.[2] However, catalytic rates obtained in the electrocatalytic oxidation of ethanol are generally sluggish; it is of importance that they are increased. Various Pt–transition-metal alloy nanoparticles have been researched with regard to their performance in the ethanol oxidation, and Pt–Sn catalysts have been widely known.[3,4] Carbon monoxide (CO) is one of several intermediates that are generated when ethanol is oxidized. CO is strongly adsorbed on the Pt atoms due to the overlap considerations between the Pt and CO orbitals, resulting in the inhibition of further oxidation reactions.[5-7] In the Pt–Sn system, Sn plays a critical role in facilitating the oxidation of CO species by transferring Sn-adsorbed oxygen-containing species to the poisoned Pt surface.[5] Although this catalytic system provides higher reaction rates and is more cost-effective, the fuel efficiency is still low. Most of the ethanol molecules are converted into acetic acid and acetaldehyde by partial oxidation (2 to 4 electrons produced per molecule of ethanol), and only small amounts of CO_2 are formed by complete oxidation (12 electrons produced per molecule of ethanol), which signifies the deterioration of fuel utilization.[8,9] According to density functional theory calculations, cleavage of the C-C bond of ethanol is the step with the highest energy barrier, therefore, CO_2, formic acid, and formaldehyde are minor products in the oxidation of ethanol.[10] To address the issue of low fuel efficiency, ternary nanoparticles additionally alloyed with Rh and Ir were recently employed, and it was found that Rh and Ir can cleave the C-C bond.[11-14] IR spectra revealed that bridge-bonded CO species are mainly formed on Rh during ethanol oxidation, suggesting that Rh is more effective than Ir in breaking the C-C bond.[15] Nonetheless, fuel efficiency and kinetics had improved, Pt-based ternary catalysts are expensive and also require complicated processes. Binary catalysts that avoid the use of Pt have been proposed in an alkaline system where the overpotentials are much smaller, however, these materials that promote the fuel efficiency via C-C bond splitting have not been reported.[15,16] Furthermore, both Rh and Sn have been only focused on promotional effect toward ethanol oxidation, because even phase-controlled nanoparticles with high-index facets exhibited too poor activities.[13,16-22]

Herein we introduce that electronic modification of the Rh–Sn nanoparticles remarkably improves the kinetics toward electrocatalytic oxidation of ethanol in an alkaline electrolyte and that the catalyst remains active at high concentrations of ethanol. These binary catalysts achieve outstanding catalytic properties and durability with ethanol C-C bond splitting. Uniform Rh–Sn nanoparticles are readily synthesized using a microwave-assisted reaction; no surfactant is required, which inhibits the access of reactants owing to the adsorption of organic molecules onto the active sites, thus synthesis and post-treatment procedure can be simplified.[23]

Polarization curves for the oxidation of ethanol on various electrocatalysts were acquired in 0.5 M and 6.0 M ethanol electrolytes (Figure 1a). Carbon-supported Sn nanoparticles display negligible reactivity, which means that Sn on its own cannot effect the oxidation of ethanol. Likewise, Rh in the absence of Sn also shows a poor activity. Interestingly, the Rh–Sn nanoparticles are highly active for the electrocatalytic oxidation of ethanol. The electrocatalytic activities were increased and the onset potentials

[a] Green City Technology Institute, Korea Institute of Science and Technology, Seoul, 136-791, Korea.
[b] Fuel Cell Research Center, Korea Institute of Science and Technology, Seoul, 136-791, Korea. E-mail: ysj@kist.re.kr; Fax: 82-2-958-5199; Tel: 82-2-958-5260
[c] School of Chemical and Biological Engineering, Seoul National University, Seoul, 151-742, Korea. E-mail: ysung@snu.ac.kr; Fax: 82-2-888-1604; Tel: 82-2-880-1889
[d] Center for Nanoparticle Research, Institute for Basic Science, Seoul, 151-742, Korea.

† Electronic Supplementary Information (ESI) available: Experimental details, cyclic voltammetry, chronoamperometry, electrochemical analysis, HR-TEM images, particle size distribution and *in situ* ATR-FTIR data. See DOI: 10.1039/x0xx00000x

were shifted to lower with increasing Sn content in Rh-Sn catalysts. Negative shift in onset potentials is the result of bifunctional mechanism.[4,24] Since the hydroxyl groups are easily formed on the Sn surface at lower potentials, increased Sn surface leads to the increasing amounts of adsorbed hydroxyl groups and more often transferred to the poisoned Rh active sites. More surprising results were encountered in 6.0 M ethanol solution, a concentration at which most catalysts are deactivated because of the excessive adsorption of CO intermediates and insufficient access of hydroxyl groups on the catalytic sites. Conventional catalysts usually suffer from a decrease in activity when the concentration of ethanol increases above 2 M,[25,26] while Rh_3Sn_7/C catalyst exhibits a significantly high current density even in 6.0 M fuel electrolyte. This is very attractive from a commercial perspective, because highly active and endurable catalysts can lead to a significant reduction in volume and weight of the system. The ratios of the forward and backward peak current densities (Figure S1) provide information on the CO tolerance of the catalysts; higher ratios correspond to greater tolerance to CO intermediates.[27] From the calculation, the ratios increase with increasing Sn content. The ratios of monometallic catalysts had lower than 1.0, while those of Rh_3Sn_7/C were considerably enhanced to 8.42 and 6.13 in 0.5 M and 6.0 M ethanol electrolyte, respectively. Electrochemical surface areas calculated from carbon monoxide displacement method of commercial Pt/C, Rh/C, Rh_9Sn_1/C, Rh_6Sn_4/C and Rh_3Sn_7/C were 40.3, 28.9, 37.2, 49.0 and 37.2 m^2/g, respectively.[28] Chronoamperometry (Figure S3) was conducted at a constant potential of 0.3 V for 1 hour to assess the durability of the catalysts, and a substantially high steady-state current density was observed for Rh_3Sn_7/C. Higher steady-state current density can be also observed in comparison with fresh Pt/C catalyst, although the activity was diminished after accelerated stability test (Figure S4). Initial and steady-state activities were summarized and compared with those of Pt/C (Figure 1b). Not only did we obtain high initial current densities, but they are also maintained at the steady state. It represents Rh_3Sn_7/C exhibits a highly active and durable electrochemical performances for the oxidation of ethanol even in high concentrations of fuel. These characteristics are attributed to faster charge-transfer kinetics and lower overpotentials. For both ethanol solutions, overpotentials (Tafel slopes, Figure S5) calculated from the quasi-steady state curves were lower for the Rh–Sn catalysts than for the monometallic catalysts, indicating that the charge transfer kinetics were faster on bimetallic catalysts.[17] Tafel slopes of Rh-Sn catalysts were slightly increased at high concentrations of ethanol, while that of monometallic catalyst was increased up to 40%, which means that the adsorption and transfer of hydroxyl groups are enough to oxidize adsorbed CO intermediates on bimetallic nanoparticles. This can be attributed to abundant Sn atoms where the hydroxyl groups are prone to adsorb. The reaction rates (Figure 1c) were also determined from the relationship between the concentration and the current density according to the Butler-Volmer equation.[29] The slopes of Rh catalysts decrease sharply when the concentration of ethanol rises above 0.1 M, whereas those of the Rh–Sn catalysts increase with an increase in the concentration of ethanol. Especially, Rh_3Sn_7/C maintains a positive slope even at high concentrations of ethanol, which indicates that the reaction rates of the intermediates have enhanced relative to other catalysts.

The morphology of the electrochemically most active catalyst Rh_3Sn_7/C was investigated (Figure 2a) using high-resolution transmission electron microscopy (HR-TEM) combined with energy-dispersive X-ray spectroscopy (EDS). A uniform distribution of metallic nanoparticles on the surface of carbon support was accomplished using a surfactant-free microwave-assisted method. Since a lot of defects and functional groups adsorbed on the surface of carbon support are served as stabilizing agents, it could be possible to attain highly uniform nanoparticles without any organic molecules. Furthermore, microwave irradiation enables the swift and simultaneous nucleation of reactive precursors by subsequent heating mechanism.[23] It could be also beneficial for obtaining the uniformity of nanoparticles that ethylene glycol as a solvent can efficiently absorb microwave energy and convert into heat, which has the highest loss tangent value among various solvents. The loss tangent is expressed as the ratio of dielectric loss and dielectric constant, which implies the ability of a solvent to convert electromagnetic energy into heat. The average particle size of Rh_3Sn_7/C was approximately 3.0 nm, and nanoparticles had slightly faded relative to monometallic catalysts due to the deformation of crystal structure between face-centered cubic structure (Rh) and tetragonal structure (Sn) and defects of oxidized surface (Figure S6). EDS results demonstrated that Rh and Sn atoms co-exist in the nanoparticles (Rh, 22.3 %; Sn, 77.7 %). With regard to the X-ray diffraction (XRD) experiments, the diffraction peaks of Rh were negatively shifted without separation as decreasing Rh content (Figure 2b). This is due to the formation of an alloy with Sn; the lattice expands because of the larger lattice distance of Sn.[30,31] Since Sn is reluctant to form wide solid solutions with Rh, heterogeneous Rh–Sn nanoparticles are formed via microwave-assisted reaction without any surfactants.

In order to elucidate the composition and the chemical state of the Rh–Sn nanoparticles in detail, high-resolution X-ray photoelectron spectroscopy (HR-XPS) employing two incident photon energies was used. Based on the universal curve, the surface-sensitive information and bulk-dominant property can be attained separately by controlling the incident photon energies.[32] The XPS peaks of Rh 3d (Figure 2c) and Sn 3d (Figure 2d) were deconvoluted to the metallic states (Rh^0 and Sn^0) and the oxidized states (Rh^{III} and Sn^{IV}). The ratios of Rh^0 in Rh/C, Rh_6Sn_4/C, and Rh_3Sn_7/C were found to be 77.6, 98.9, and 84.9%, respectively, when an incident photon energy of 630 eV was used, whereas they were found to be 99.3, 97.1, and 95.2%, respectively, at 1000 eV. The Rh surface region of Rh/C is further oxidized than that of other catalysts, which is a result of the absence of lateral repulsion by hydroxyl groups adsorbed on Sn nearby Rh atom.[33] With regard to Sn, the Sn^{IV} in Rh_6Sn_4/C, Rh_3Sn_7/C, and Sn/C were found to be 95.3, 99.8, and 99.9%, respectively, when an incident photon energy of 630 eV was used (82.2, 90.8, and 92.9%, respectively, at 1000 eV). The XPS results demonstrate that metallic Rh and oxidized Sn dominate in the heterogeneous nanoparticles, and that the metallic properties are maintained well at the core part of a nanoparticle relative to the surface, which contribute to the electronic interactions between metals. The Rh 3d core-level peak of Rh–Sn/C shifts to higher energies as the Rh content increases, which is attributed to changes in the electron density of the metal and in the bonding energy between metal and adsorbed molecules, as an indicator of

alloying.[34] According to the effective-medium theory, the upshift in binding energy can be induced by a decrease in the number of neighboring Rh atoms around a single Rh atom.[35-37]

Rh K-edge of X-ray absorption near-edge spectroscopy (XANES) on the Rh-Sn catalysts was performed to indirectly estimate the shifts in electron density of metal. Peak intensities at white line increase as the Rh content decreases, which implies a concomitant decrease in the electron density at the Rh atom (Figure 3). This means that the tendency in interactions between Rh and the adsorbates strengthens on the nanoparticle, resulting in easier adsorption of ethanol molecules (relative to pure Rh, for which poor ethanol oxidation reactivity was observed in the polarization curve).[38,39] And these adsorbed CO species on Rh can be readily oxidized by abundant hydroxyl groups on nearby Sn atoms. Although spectra of Sn-abundant samples resemble to that of oxide due to the increase oxidation state of Rh evaluated from XPS depth-profile previously, up-shifts of binding energy in XPS and negative shifts in XRD demonstrate that electronic modification occurs at Rh atom coordinated by Sn atoms.[40] For the Rh-Sn electrocatalysts, therefore, the reinforced adsorption ability between metal and molecules (electronic modification) and enhanced oxidation probability on Rh surface with adjacent SnO_2 (bifunctional effect) may lead to a superior ethanol oxidation reactivity.

To evaluate the yield of the complete oxidation pathway, qualitative information about the final product as CO_2 was attained using in situ attenuated total reflection-fourier transform infrared (ATR-FTIR) measurements under electrochemical test conditions (Figure 4a).[41] The normalized CO_2 band intensity is very low for the Pt/C catalyst, which means most of the ethanol is only partially oxidized (Figure 4b, Figure S7).[8] However, intense peaks appear for the Rh_3Sn_7/C catalyst, even at low potentials, in comparison with the commercial catalyst. This indicates that the ability of the Rh_3Sn_7/C catalyst to split the ethanol C-C bond is significantly enhanced, and that the fuel efficiency has improved. Normalized CO_2 intensities were increased for the Rh-Sn catalyst at low potential regions, although the oxidation currents in cyclic voltammetry were too low. This implies that the oxidation of ethanol is unfavorable at low potential ranges, however, the probability of conversion from ethanol to CO_2 is relatively higher than conventional catalyst. According to the theoretical calculations and experimental techniques such as CO displacement, CO formation is energetically favorable on noble metal surface at low potentials, but CO_2 production is limited owing to the unavailability of oxidants.[9] In case of Rh-Sn catalysts, CO-poisoned noble metal surface can be easily cleaned by hydroxyl groups adsorbed on the nearby Sn surface. Since the Sn is likely to adsorb hydroxyl groups at low potential, and to transfer them to CO-poisoned Rh surface, which resulting in facile oxidation of CO intermediates with hydroxyl groups for bimetallic nanoparticles. These results are in accordance with the notable electrochemical activity of the Rh-Sn catalyst in the polarization curve.

Conclusions

Uniform Rh–Sn heterogeneous nanoparticles have been synthesized on a carbon support using a surfactant-free microwave-assisted method that is facile and economically viable. The bifunctional effect as well as electronic modification lead to active and durable Rh–Sn electrocatalysts for the oxidation of ethanol. These catalysts maintain their activity even at high concentrations of ethanol. Low Tafel slopes and high reaction rates are also observed even at high fuel concentrations, which allows for a significant reduction in volume and weight of the fuel cell system. Superior fuel efficiency has been achieved; more of the ethanol is completely oxidized to form CO_2. Thus the Rh–Sn catalyst has not only superior electrochemical activity and durability but also an increased fuel efficiency for the oxidation of ethanol through the combination effects of bifunctional mechanism, electronic modification, and C-C bond splitting. We expect that these results will relieve the dependence on noble metals, leading to distribution of inexpensive catalysts, and future work may focus on the modification of the nanoparticle surface and its application in fuel cell systems.

Acknowledgements

This work was supported by the Institute for Basic Science (IBS) in Korea.

Notes and references

1 A. Chen and P. Holt-Hindle, *Chem. Rev.,* 2010, **110**, 3767.
2 O. Inderwildi and D. King, *Energy Environ. Sci.,* 2009, **2**, 343.
3 W.-P. Zhou, S. Axnanda, M. G. White, R. R. Adzic and J. Hrbek, *J. Phys. Chem. C,* 2011, **115**, 16467.
4 E. Antolini and E. R. Gonzalez, *Catal. Today,* 2011, **160**, 28.
5 I. Kim, O. H. Han, S. A. Chae, Y. Paik, S.-H. Kwon, K.-S. Lee, Y.-E. Sung and H. Kim, *Angew. Chem. Int. Ed.,* 2011, **50**, 2270.
6 J. F. Gomes, K. Bergamaski, M. F. S. Pinto and P. B. Miranda, *J. Catal.,* 2013, **302**, 67.
7 R. Wang, J. Liu, P. Liu, X. Bi, X. Yan, W. Wang, X. Ge, M. Chen and Y. Ding, *Chem. Sci.,* 2014, **5**, 403.
8 M. Zhu, G. Sun and Q. Xin, *Electrochim. Acta,* 2009, **54**, 1511.
9 R. Kavanagh, X.-M. Cao, W.-F. Lin, C. Hardacre and P. Hu, *Angew. Chem. Int. Ed.,* 2012, **51**, 1572.
10 R. Alcala, M. Mavrikakis and J. A. Dumesic, *J. Catal.,* 2003, **218**, 178.
11 A. Kowal, M. Li, M. Shao, K. Sasaki, M. B. Vukmirovic, J. Zhang, N. S. Marinkovic, P. Liu, A. I. Frenkel and R. R. Adzic, *Nat. Mater.,* 2009, **8**, 325.
12 W. Du, Q. Wang, C. A. LaScala, L. Zhang, D. Su, A. I. Frenkel, V. K. Mathura and X. Teng, *J. Mater. Chem.,* 2011, **21**, 8887.
13 M. Li, D. A. Cullen, K. Sasaki, N. S. Marinkovic, K. More and R. R. Adzic, *J. Am. Chem. Soc.,* 2013, **135**, 132.
14 N. Erini, R. Loukrakpam, V. Petkov, E. A. Baranova, R. Yang, D. Teschner, Y. Huang, S. R. Brankovic and P. Strasser, *ACS Catal.,* 2014, **4**, 1859.
15 N. R. D. Tacconi, R. O. Lezna, B. Beden, F. Hahn and C. Lamy, *J. Electroanal. Chem.,* 1994, **379**, 329.
16 S. Shen and T. Zhao, *J. Mater. Chem. A,* 2013, **1**, 906.
17 W. Du, K. E. Mackenzie, D. F. Milano, N. A. Deskins, D. Su and X. Teng, *ACS Catal.,* 2012, **2**, 287.
18 N.-F. Yu, N. Tian, Z.-Y. Zhou, L. Huang, J. Xiao, Y.-H. Wen and S.-G. Sun, *Angew. Chem. Int. Ed.,* 2014, **53**, 5097.
19 Z. Zhang, J. Liu, J. Gu, L. Su and L. Cheng, *Energy Environ. Sci.,* 2014, **7**, 2535.
20 S. Axnanda, W.-P. Zhou and M. G. White, *Phys. Chem. Chem. Phys.,* 2012, **14**, 10207.

21 Y. W. Lee, M. Kim, S. W. Kang and S. W. Han, *Angew. Chem. Int. Ed.,* 2011, **50**, 3466.
22 L. Rao, Y.-X. Jiang, B.-W. Zhang, Y.-R. Cai and S.-G. Sun, *Phys. Chem. Chem. Phys.,* 2014, **16**, 13662.
23 M. Baghbanzadeh, L. Carbone, P. D. Cozzoli and C. O. Kappe, *Angew. Chem. Int. Ed.,* 2011, **50**, 11312.
24 P. A. Russo, M. Ahn, Y.-E. Sung and N. Pinna, *RSC Adv.,* 2013, **3**, 7001.
25 Z. X. Liang, T. S. Zhao, J. B. Xu and L. D. Zhu, *Electrochim. Acta,* 2009, **54**, 2203.
26 L. Ma, D. Chu and R. Chen, *Int. J. Hydrogen Energy,* 2012, **37**, 11185.
27 M. Arenz, V. Stamenkovic, B. B. Blizanac, K. J. Mayrhofer, N. M. Markovic and P. N. Ross, *J. Catal.,* 2005, **232**, 402.
28 Q.-S. Chen, F. J. Vidal-Iglesias, J. Solla-Gullon, S.-G. Sun and J. M. Feliu, *Chem. Sci.,* 2012, **3**, 136.
29 A. J. Bard and L. R. Faulkner, Electrochemical methods: Fundamentals and applications, John Wiley & Sons, Inc., 2001.
30 R. F. B. De Souza, L. S. Parreira, D. C. Rascio, J. C. M. Silva, E. Teixeira-Neto, M. L. Calegaro, E. V. Spinace, A. O. Neto and M. C. Santos, *J. Power Sources,* 2010, **195**, 1589.
31 M. Li, A. Kowal, K. Sasaki, N. Marinkovic, D. Su, E. Korach, P. Liu and R. R. Adzic, *Eletrochim. Acta,* 2010, **55**, 4331.
32 M. P. Seah and W. A. Dench, *Surf. Interf. Anal.,* 1979, **1**, 2.
33 J. Zhang, M. B. Vukmirovic, K. Sasaki, A. U. Nilekar, M. Mavrikakis and R. R. Adzic, *J. Am. Chem. Soc.,* 2005, **127**, 12480.
34 M. Wakisaka, S. Mitsui, Y. Hirose, K. Kawashima, H. Uchida and M. Watanabe, *J. Phys. Chem. B,* 2006, **110**, 23489.
35 B. Hammer and J. K. Norskov, *Adv. Catal.,* 2000, **45**, 71.
36 M. V. Ganduglia-Pirovano, V. Natoli, M. H. Cohen, J. Kudrnovsky and I. Turek, *Phys. Rev. B,* 1996, **54**, 8892.
37 J. K. Norskov, K. W. Jacobsen, P. Stoltze and L. B. Hansen, *Surf. Sci.,* 1993, **283**, 277.
38 N. Jung, D. Y. Chung, J. Ryu, S. J. Yoo and Y.-E. Sung, *Nano Today,* 2014, **9**, 433.
39 Z.-F. Xu and Y. Wang, *J. Phys. Chem. C,* 2011, **115**, 20565.
40 T. Ikeda, A. Xiong, T. Yoshinaga, K. Maeda, K. Domen and T. Teranishi, *J. Phys. Chem. C,* 2013, **117**, 2467.
41 T. Sato, K. Kunimatsu, K. Okaya, H. Yano, M. Watanabe and H. Uchida, *Energy Environ. Sci.,* 2011, **4**, 433.

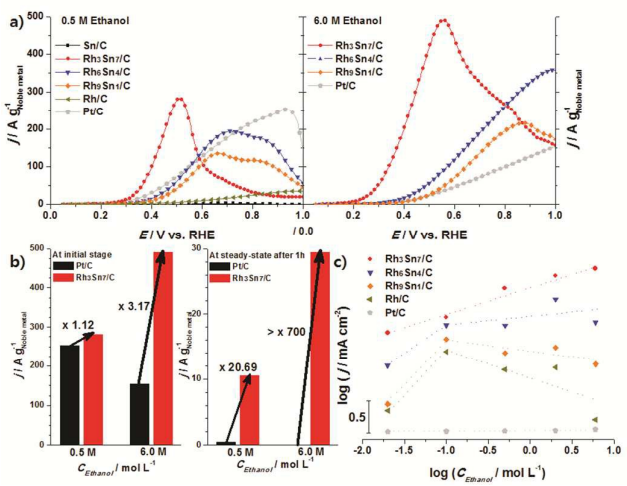

Figure 1. a) Voltammetric profiles for the electrocatalytic oxidation of ethanol in an oxygen-free solution containing 0.1 M potassium hydroxide and (left) 0.5 M or (right) 6.0 M ethanol at a scan rate of 20 mV s^{-1}. b) Current densities of commercial Pt/C and of Rh_3Sn_7/C in 0.5 M and 6.0 M ethanol electrolytes, at the initial stage and after application of a constant potential of 0.3 V for 1 hour (chronoamperometry). c) Plot of log(current density) versus log(ethanol concentration) of Rh-Sn catalysts and Pt catalyst in 0.5 M ethanol electrolyte at 0.4 V with a scan rate of 1 mV s^{-1}.

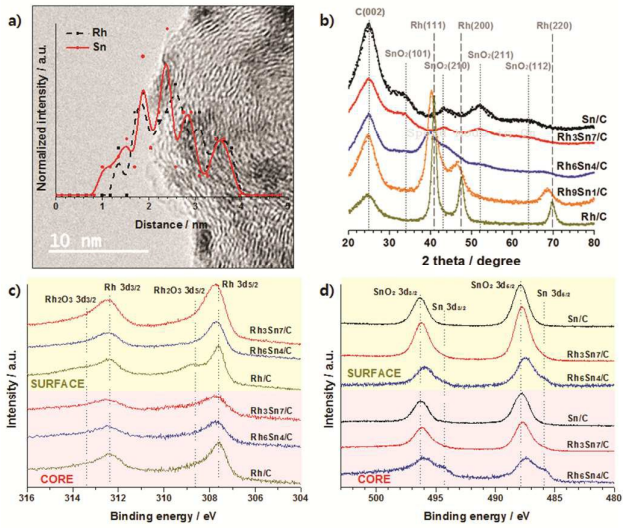

Figure 2. a) High-magnification TEM images of heterogeneous Rh_3Sn_7 nanoparticles supported on carbon, and line-scanning results for an nanoparticle. b) HR-XRD patterns of Rh/C, Sn/C, and Rh–Sn catalysts with indicators for crystal structures. c) Rh 3d and d) Sn 3d HR-XPS spectra with depth profiles.

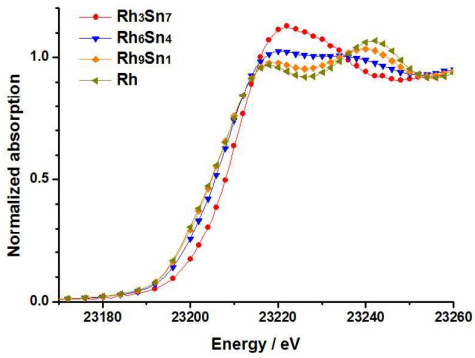

Figure 3. Rh K-edge of XANES spectra of Rh-Sn catalysts.

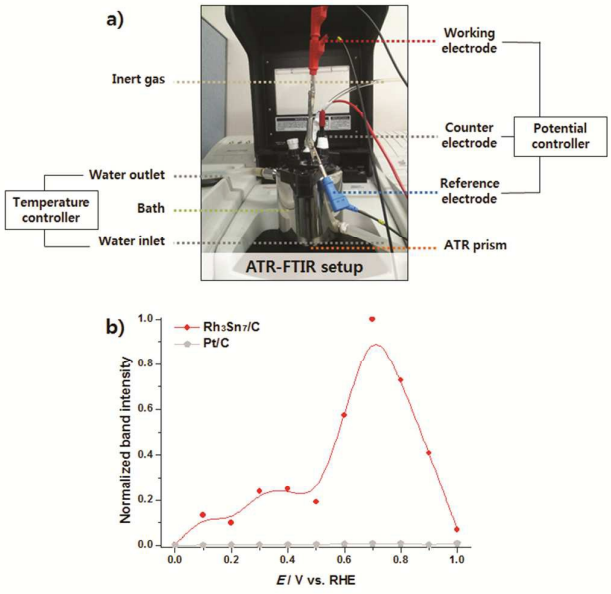

Figure 4. a) *in situ* ATR-FTIR measurements and b) normalized IR intensities (2343 cm^{-1}, asymmetric stretch of CO_2) on Pt/C and Rh_3Sn_7/C during electrocatalytic oxidation of ethanol, employing a potential sweep in 0.5 M ethanol electrolyte at a scan rate of 20 mV s^{-1}.